IEEE Transactions on Industrial Informatics, Volume 16, Issue 7, July 2020, pp. 4592-4602
DOI: 10.1109/TII.2019.2950808

Inversion Technique for Quantitative Infrared Thermography Evaluation of Delamination Defects in Multilayered Structures

Haochen Liu, Cuixiang Pei, Shejuan Xie, Yong Li, *Senior Member, IEEE*, Yifan Zhao, *Senior Member, IEEE,* and Zhenmao Chen*

***Abstract*—Inverse analysis is a promising tool for quantitative evaluation offering informative model-based prediction and providing accurate reconstruction results without pre-inspections for characterization criteria. For traditional defect inverse reconstruction, a large number of parameters are required to reconstruct a complex defect, and the corresponding forward modelling simulation is very time-consuming. Such issues result in ill-posed and complex inverse reconstruction results, which further reduces its practical applicability. In this paper, we propose and experimentally validate an inversion technique for the reconstruction of complexly-shaped delamination defects in a multilayered metallic structure using signals derived from infrared thermography (IRT) testing. First, we employ a novel defect parameterization strategy based on Fourier series fitting to represent the profile of a complicated delamination defect with relatively few coefficients. Secondly, the multi-medium element modelling method is applied to enhance a FEM fast forward simulator, in order to solve the mismatching mesh issue for mesh updating during inversion. Thirdly, a deterministic inverse algorithm based on a penalty conjugate gradient algorithm is employed to realize a robust and efficient inverse analysis. By reconstructing delamination profiles with both numerically-simulated IRT signals and those obtained through laser IRT experiments, the validity, efficiency and robustness of the proposed inversion method are demonstrated for delamination defects in a double-layered plate. Based on this strategy, not only is the feasibility of the proposed method in Infrared thermography NDT validated, but the practical applicability of inversion reconstruction analysis is significantly improved.**

***Index Terms*—Infrared thermography testing, Multilayered structure, Delamination profile, Quantitative nondestructive evaluation, Inverse analysis.**

I. Introduction

Component quality and structural integrity have caused significant health and safety concerns in industry, with respect to maintenance and through-life engineering [1, 2]. Nondestructive testing and evaluation (NDT&E) is a powerful technique to diagnose damage and degradation caused by operational and environmental factors, and provides abundant results of defect information in both the pre-service and in-service periods [3-5]. Bai *et al.* proposed a saliency-based defect detection method based on scanning electronic microscope images of electronic chips or dies in semiconductor production lines [6]. Piciarelli *et al.* developed a visually-based software system to assist inspectors in internal diagnosis of pipeline infrastructure [7]. Visual and optical inspection are intuitive in character, but can only detect surface flaws [8, 9]. Eddy current testing offers high detection efficiency, but is limited by its inapplicability to non-conductive materials [10]. Ultrasonic testing can perform deep accurate detection, but has a surface blind region and requires a coupling agent [11, 12]. Similarly, radiography testing presents safety and cost issues, while magnetic particle testing is only suitable for ferromagnetic materials [13]. Because of their own limitations, these NDT&E techniques are not applicable for those applications which simultaneously demand detection of internal defects by a non-contact, low-cost method.

Welded multilayered structures, due to their capabilities of high-intensity structure, good thermal conductivity and corrosion and radiation resistance, are widely used in the nuclear power, military and chemical industries. During the fabrication and servicing of multilayered structures, such defects as delamination and disbonding may occur at the bonding surface due to thermal stress, radiative fatigue, insufficient welding or other causes [14, 15]. Delamination defects may reduce structural strength, worsen heat transfer capability and cause irreparable failure. Therefore, it is of great

Manuscript received June 28, 2019; revised August 12, 2019; accepted October 07, 2019. This work was supported in part by the National Key Research and Development Program of China under Grant 2017YFF0209703, in part by the Natural Science Foundation of China under Grand (11927801, 51577139, 51877163) and in part by the Xinjiang Natural Science Foundation under Grant 2019D01A76. (*Corresponding authors*: Zhenmao Chen.)

Haochen Liu is with the State Key Laboratory for Strength and Vibration of Mechanical Structures, School of Aerospace, Xi'an Jiaotong University, 28 West Xianning Road, Xi'an, China, and also with the School of Aerospace, Transport and Manufacturing, Cranfield University, Bedfordshire MK43 0AL, U.K. (e-mail: haochen.liu@cranfield.ac.uk;)

Cuixiang Pei, Shejuan Xie, Yong Li and Zhenmao Chen are with the State Key Laboratory for Strength and Vibration of Mechanical Structures, School of Aerospace, Xi'an Jiaotong University, 28 West Xianning Road, Xi'an, China. (e-mail: pei.cx@mail.xjtu.edu.cn; xiesj2014@mail.xjtu.edu.cn; yong.li@mail.xjtu.edu.cn; chenzm@mail.xjtu.edu.cn).

Yifan Zhao are with the School of Aerospace, Transport and Manufacturing, Cranfield University, Bedfordshire MK43 0AL, U.K. (e-mail: yifan.zhao@cranfield.ac.uk).

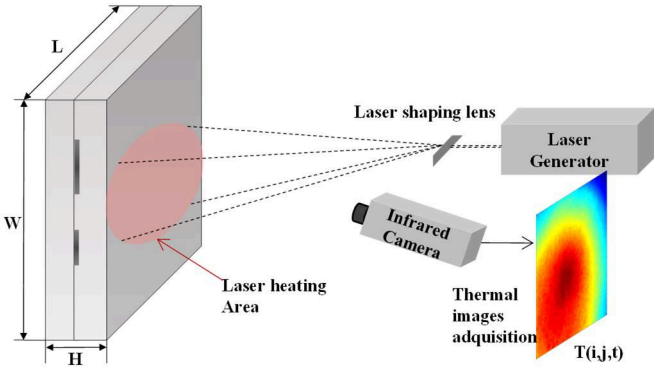

Fig. 1. Principle of laser infrared thermography NDT system

significance to detect the delamination defect nondestructively during both its manufacturing and servicing in order to ensure the quality of the multilayered structures as a whole.

Infrared thermography (IRT) is a powerful NDT technique that offers rapid, non-contact, robust non-invasive inspection and real-time monitoring. With many effective applications in nondestructive evaluation (NDE), quality control, condition monitoring and fault diagnosis, it has been attracting widening attention over recent decades. IRT employs the heat flow analysis and temperature imaging techniques to detect defects, anomalies and failures. Thermography can be divided into two modes, i.e. active and passive thermography, which are distinguished by whether or not the thermal flow in the inspection target is generated by external excitation energy. Active IRT employs external sources to heat the specimen, and the laser is ideal for remote-inspection of delamination defects in multilayered structures, as it offering easy control, high concentration and precise directionality of excitation. Compared to flash lamps, the laser provides dominant performance in energy density, intensity, accuracy and adjustability. By contrast, the laser is superior to eddy current thermography in remote heating capability, due to its low attenuation, especially in applications where the induction coil is inaccessible to the object. For delamination in multi-layered metallic structures, the high energy and readily controllable laser spot provides better heating uniformity and a higher temperature signal to noise ratio. These are crucial to achieve a precise defect quantitative evaluation. Hence, laser thermography, as shown in Fig. 1, and its varied forms has been applied in many NDE scenarios such as, welds [16] and surface evaluation [17], mechanical equipment [18], composites structures etc. [19, 20].

Equipped with a powerful inspection technique, a defect evaluation or quantification is of great significance for lifetime assessment and maintenance management in through-life engineering. In IRT NDE, methods based on image processing are in common use, from the basic of dealing with fixed pattern noise, and the thermal contrast algorithm, to the thermography signal reconstruction (TSR) algorithm [21]. The defect evaluation results based on these methods are highly dependent on the quantitative parameters used in the algorithm. The task commonly demands numerous standardized specimen pretests and calibrations to define the appropriate parameters. Moreover the quantification accuracy may vary according to the material, structure and varied levels of experience of different operators. In any case, this kind of method is inadequate for quantification

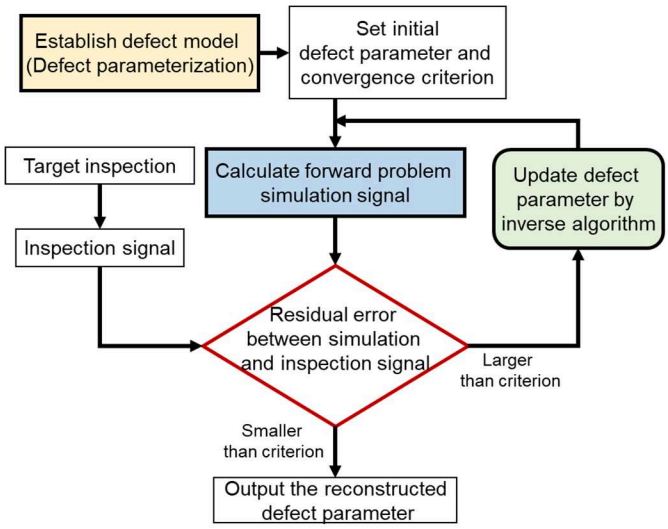

Fig. 2. Work flow of defect reconstruction by inverse analysis

of multiple defect parameter. For example, when both defect size and conductivity parameters need to be quantified simultaneously.

Fortunately, as an alternative and more effective strategy, defect reconstruction based on inverse analysis and inspection signals is capable of outputting reliable results in complicated defect evaluation cases. In inversion NDE, the forward problem refers to the analysis of acquiring the inspection signal with known defect information, which can be realized by simulation method. The inverse problem refers to the reconstruction of the unknown defect information from the inspection signal, which can be achieved by an inverse algorithm (i.e. optimization methods).

The workflow of typical defect reconstruction by inverse analysis can be seen diagramed in Fig.2. Initially, it is essential to establish a defect model and forward problem simulation method. The objective function is then constructed as the residual error between the experimental and simulated signal. By searching the optimal parameters with the optimization algorithm in the defect parameters space to minimize the residual error, the defect model can be modified and updated to approximate the real defect. The defect model, forward problem simulation and inverse algorithm are the three main components in NDE inversion, and have attracted many researchers in different application areas.

Several studies have presented applications of inverse analysis based on a variety of techniques for reconstruction of multiple kinds of defect information, including wall-thinning depth [22], crack geometry, defect volume [23] and material thermal property [24]. In IRT NDE, the inverse reconstruction approach has been proven to be effective in measurement of corrosion depth and delamination size and depth [25]. But the models used in these researches are oversimplified by the assumption that the defect has a regular shape, which is unsuitable for sizing a complex delamination profile.

In addition, a few studies focus on reconstruction of complex defect geometry. Richter *et al.* proposed a thermography-based reconstruction method of back wall geometry using the Levenberg–Marquardt method [26]. Chen *et al.* [27] and Xie *et al.* [22] proposed different complex shape parameterization models based on inverse eddy current NDE techniques for crack

and wall-thinning based on deterministic, stochastic and hybrid inversion algorithms. To obtain the reconstruction of a complex geometry profile, these approaches represent the profile with too many parameters or are too highly dependent on model meshing, which results in a high computational burden and inverse complexity. In metallic welded multi-layered structure, delamination commonly happens at and propagates along the very thin material interfaces, which affects the structural integrity significantly. A planar complex 2D profile is forensic and provides useful indications of delamination propagation, which in turn draws more attentions to the issues of life assessment and maintenance. Therefore, an accurate and efficient inversion technique for complex delamination 2D profile reconstruction is constructive and eagerly required.

Based on the above analysis, the contributions of this work lie in the development of an inversion technique for delamination profile reconstruction, which consists of an updated fast forward simulation, a new profile parameterization strategy, and a corresponding robust inversion algorithm.

1) The updated fast forward simulation gives both a fast forward signal calculation and a solution for the mesh mismatching problem caused by complexly-shaped defect. Not only the efficiency of the entire reconstruction process is greatly improved, but also the accuracy of sizing complex profile can be improved.

2) Following the new profile parameterizing strategy can describe the complex profile with only a small number of defect parameters, which significantly advances the practical applicability of inverse reconstruction. Without losing sizing accuracy, reconstructing a small number of defect parameters offers the inversion analysis with fewer problems of ill-posedness, and less waste of time.

3) In addition, we proposed the use of a penalty function conjugate gradient (CG) algorithm based on the new defect parameterization and forward simulation, which guarantees a robust and efficient convergence under model constraint conditions. The algorithm also ensures a stability convergence for inversion analysis. Finally, through reconstruction cases based on simulated and experimental signals, the proposed technique is validated.

This paper is organized as follows: the fast forward simulator proposed by authors is briefly stated in Section II, with the addition of a multi-medium modelling method to improve the forward simulation. In Section III, we proposed a new defect parameterization strategy for sizing delamination of a complex profile and the corresponding inversion numerical algorithm. The validations of the reconstruction method are given in Section IV using both the simulated IRT signals and those obtained through experiments. Finally, the conclusions are given in Section V.

II. Forward Analysis Method for IRT Problem

In the inversion analysis, a large amount of accurate forward analysis is indispensable, whether both for a model-based or a model-free reconstruction. In this research, a model-based forward problem simulation is adopted. However, since using a priori meshed model in forward analysis, a mesh mismatching problem would inevitably occur due to the intractable updated defect profile crossing the original mesh. In addition, use of a conventional three dimensional (3D) model problem simulation solver leads to excessive computational time expanded on multiple iterations in inversion analysis. In order to overcome these difficulties, two following approaches are applied to the forward problem.

A. Multi-medium Element (MME) Modelling

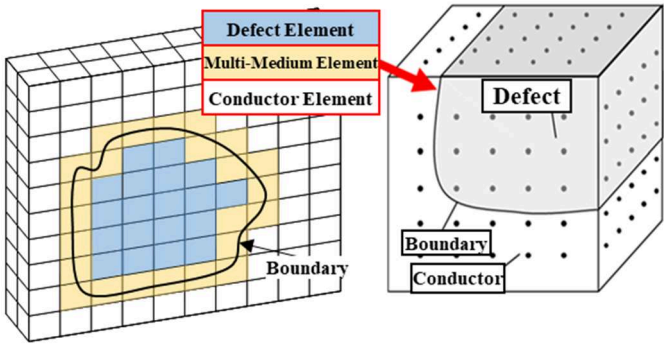

Fig. 3. Principle of Multi-medium Element Modeling

In the inversion analysis, the updated complex defect profile commonly passes through the original element grid, which often worsens the forward problem accuracy in the next reconstruction step. Generating a new fine mesh according to the updated profile is a common solution to this issue. However, this would obviously slow down the reconstruction and result in a different calculation error level at each reconstruction step. Therefore, in order to improve the applicability of the original mesh, a multi-medium element modeling approach is introduced as follow.

In FEM modeling, the Gauss integrating points in each element are the essential unit used to calculate the element stiffness matrix. The MME modeling is intended to solve the key issue of material attribution at each Gauss integrating point when the complex profile passes through the element [30, 31]. As shown in Fig. 3, with the MME, all the elements are classified into three categories according to the defect profile, which includes defect elements (DE), conductor elements (CE), and multi-medium elements containing both materials.

The element stiffness matrix coefficients can be conducted by integration equation (1),

$$\begin{aligned} [K]_e &= \kappa \sum_i w_i \cdot B^{'}(r_i)^T \cdot \nabla N(r_i) \\ [C]_e &= \rho c \sum_i w_i \cdot N(r_i) \cdot N(r_i)^T, \quad i = 1,\ldots, N_{Guass\ points} \end{aligned} \tag{1}$$

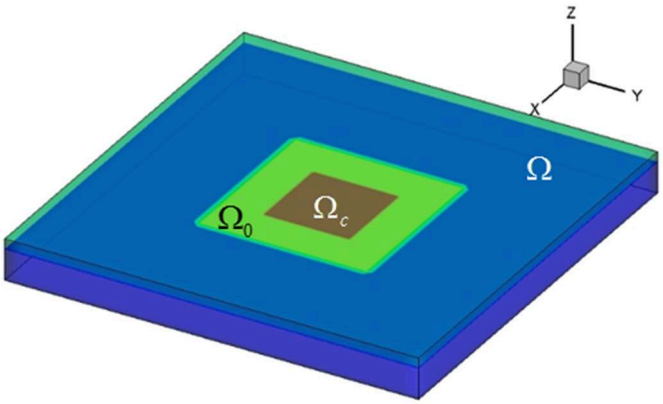

Fig. 4. Definition of analysis regions of the fast forward solver

where, $[K]_e$ and $[C]_e$ are coefficients of each element. r_i is the location vector of the *i-th* Gauss point.

Due to the various materials existing in MME, the distribution of the various material parameters has to be considered when generating the element coefficient matrix of the MME. In other words, the element coefficients $[K]_e$ and $[C]_e$ obtained by equation (1) depends on the location of the Gauss point: i.e., if one Gauss point is within the defect profile, the defect material property will be used in (1) for this point. Otherwise, the conductor material property will be adopted. If the number of Gauss points adopted is sufficient, the element coefficient can be calculated with high precision. After calculation and comparison accuracy, the number of $7\times7\times7$ Gauss points in each 3D element is sufficient for high-accuracy calculation. Using the aforementioned theory, with MME modeling, the issue of mismatching mesh can be properly solved and the original mesh can be used in the whole reconstruction process.

B. Proposed Fast Forward Problem Simulator

After modeling, a proposed fast forward thermography signal simulation tool is briefly introduced [29]. The governing equation of the pulse thermography (PT) problem can be written as (2). By using Fourier transformation, the response signal can be calculated, based on the frequency domain summation method. The transformed FEM governing equations are presented as (3),

$$[K]\{T(t)\}+[C]\left\{\frac{\partial T(t)}{\partial t}\right\}=\{Q(t)\} \tag{2}$$

$$\sum_{n=0}^{N}\left([K]+j\omega_n[C]\right)\{\tilde{T}_n\}e^{j\omega_n t}=\sum_{n=0}^{N}\{\tilde{Q}_n\}e^{j\omega_n t}$$
$$\left([K]+j\omega_n[C]\right)\{\tilde{T}_n\}=\{\tilde{Q}_n\},\ n=0,1,2,3,4..... \tag{3}$$

where $\{Q\}$ denotes the excitation heat source and $[K]$, $[C]$ are the coefficient matrices of the FEM equations. To guarantee the precision and enhance the efficiency, two strategies are applied. First, the number of necessary harmonic frequency components is reduced by using an interpolation strategy [28]. Secondly, a fast forward scheme based on the databases strategy is applied to realize the rapid calculation of the temperature perturbation caused by a delamination defect [29].

A numerical model of the thermography problem is shown in Fig. 4. The symbol Ω denotes the whole no-defect object, Ω_c is the region of delamination; and Ω_0 denotes a selected suspect region that contains the delamination. To approximate realistic cracks, Ω_0 is chosen as a planar region with a thickness equal to the delamination. The fast forward scheme based on the databases strategy can be described as follows using this numerical model.

Upon subtracting the single-frequency IRT governing equation for the unflawed model from the single-frequency governing equation for the flawed model, one can obtain the governing equations about the field perturbation T^f for single-frequency IRT problems. After separately denoting all the nodes as three parts, the FEM equations of the IRT problem become (4)

$$\begin{bmatrix}\bar{K}_{11}&\bar{K}_{12}&\bar{K}_{13}\\ \bar{K}_{21}&\bar{K}_{22}&\bar{K}_{23}\\ \bar{K}_{31}&\bar{K}_{32}&\bar{K}_{33}\end{bmatrix}\begin{Bmatrix}T_1^f\\T_2^f\\T_3^f\end{Bmatrix}=\begin{bmatrix}\tilde{K}_{11}&0&0\\0&0&0\\0&0&0\end{bmatrix}\begin{Bmatrix}T_1^f+T_1^0\\T_2^f+T_2^0\\T_3^f+T_3^0\end{Bmatrix} \tag{4}$$

where $[\bar{K}]$ is the FEM discrete coefficient matrix of the flawless model, $[\tilde{K}_{11}]$ the coefficient matrix corresponding to the defect model, $\{T_1\}$ the temperature at the nodes of delamination elements, $\{T_3\}$ the inspection surface nodes and $\{T_2\}$ is the remaining unknowns. By denoting the inverse matrix of $[\bar{K}]$ as $[H]$, the following equation (5), correlating the unflawed model to the defect perturbation field in Ω_c, and the surface perturbation field response can be derived by (6).

$$\left[I-H_{11}\tilde{K}_{11}\right]\{T_1^f\}=[H_{11}]\left[\tilde{K}_{11}\right]\{T_1^0\} \tag{5}$$

$$\{T_3^f\}=\left[H_{31}\tilde{K}_{11}\right]\{T_1^f+T_1^0\} \tag{6}$$

Since the coefficient matrices $[H_{11}]$, $[H_{31}]$ and temperature vector $\{T_1^0\}$, $\{T_3^0\}$ are independent of the defect geometry, once they have been calculated a priori and stored as databases, there is no need to recalculate for defects of different profiles. Thus, the fast forward scheme can significantly promote simulation efficiency by greatly reducing the dimension of governing equations. The particular fast forward scheme proposed by the authors is carefully discussed in [29].

The fast numerical scheme shown in (4) mainly focus on response perturbation between the delaminated model and sound model caused by an inner defect. The scheme is suitable for heat sources such as the laser and flash lamp. Currently, it is not suitable for an inner source problem such as the eddy current pulsed thermography. In addition, for a composite material, the anisotropic property has to be considered when using equation (4). However, there is big potential to update (4) for eddy current heating by solving eddy current heating with the database strategy and for composite material using anisotropic thermal conductivity, which will be studied in future work.

III. Theory and Methodology for Inverse Analysis

The principle of delamination profile sizing by inversion analysis is shown in Fig.2, and consists of three components: defect parameterization, forward problem simulation and inversion algorithm. These components are all crucial to the inverse reconstruction analysis, each impacting on sizing accuracy, inversion robustness and reconstruction efficiency.

A. Delamination profile parameterization method

A profile parameterizing method is a way of describing the geometrical profile of a defect with modelling parameters. A wise parameterizing strategy is not only applicable to wide variety of complex geometrical profiles, while guaranteeing good sizing accuracy, but also improves reconstruction efficiency and decreases the complexity of inverse analysis. Several authors have proposed different parameterizing strategies for representing complexly-shaped defects.

Xie *et al.* proposed a stepwise shaped approximation method to describe the profile of wall thinning. [22]. It approximates

the complex profile as a group of slit defects of given width but of differing length and parameterized them with a set of horizontal slits with differing numbers of elements. Consequently, the sizing accuracy based on this approach is heavily dependent on the grid size which generates a large number of parameters. Chen *et al.* proposed a piecewise line parameterizing strategy using discrete points to represent the depth profile of a crack [27]. This method parameterizes the profile with the coordinates of the discrete points. However, this strategy also leads to a highly complex inverse sizing, which requires many defect parameters to be quantified. Therefore, in this section, a new profile parameterizing method for delamination profile is proposed.

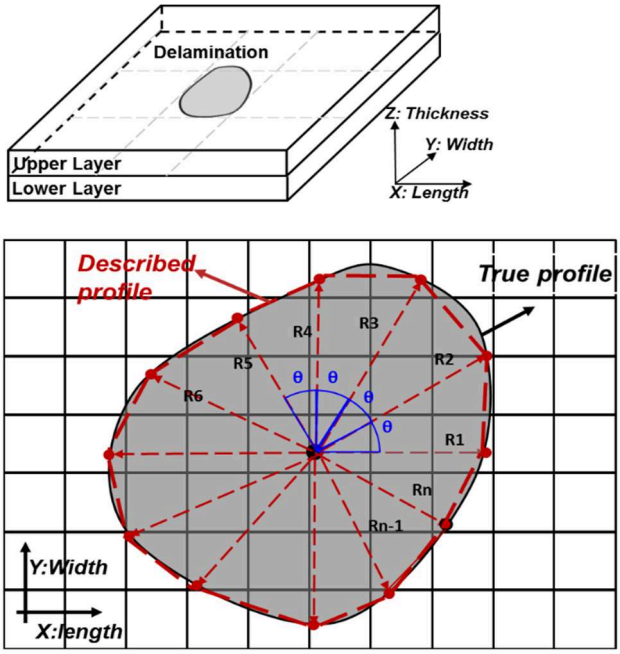

Fig. 5. Radiative radius approximation for complex delamination profile

Fig. 5 shows a common form of delamination in a double-layered structure with complex and irregular profile. Because of the closed-circumferential feature of delamination profile in XY planar, a circumferential radiative radius strategy presented below is suitable to describe the complex profile. At the beginning, a fixed inner point is selected inside the closed profile. Then, launching from the fixed inner point, a group of radiative radiuses are used to approximate the defect boundary. When the number of radiuses tends to infinite, the profile is accurately approximated by the end points of radiuses. In other words, the defect profile is equivalent to the trail of radius ends when a variable radius continuously sweeps the perigon from 0 to 2π.

Pursuing this radiative radius strategy, a Fourier series fitting method is proposed to describe the defect shape. As shown in Fig. 6, the profile is then represented by $R(x, \theta)$, which is the length of the variable sweeping radius. x is the defect parameters vector, θ is the angle of radius departure from the X-axis. To parameterize the function $R(x, \theta)$, a polynomial model based on Fourier series fitting method is applied and shown in (7).

$$R(x,\theta) = \frac{1}{2}x_0 + x_n\sum_{n=1}^{N}\cos(n\theta) + \varepsilon(\theta), \quad \theta \in [0, 2\pi] \tag{7}$$

$$\textit{Constraint conditions}: \ Rmax > R(x,\theta) > 0$$

where N is the model order, $\varepsilon(\theta)$ is the high-order noise and A_0 and A_n are Fourier series coefficients representing the $R(x, \theta)$. Hence, the complex delamination profile is eventually parameterized to the Fourier series coefficients.

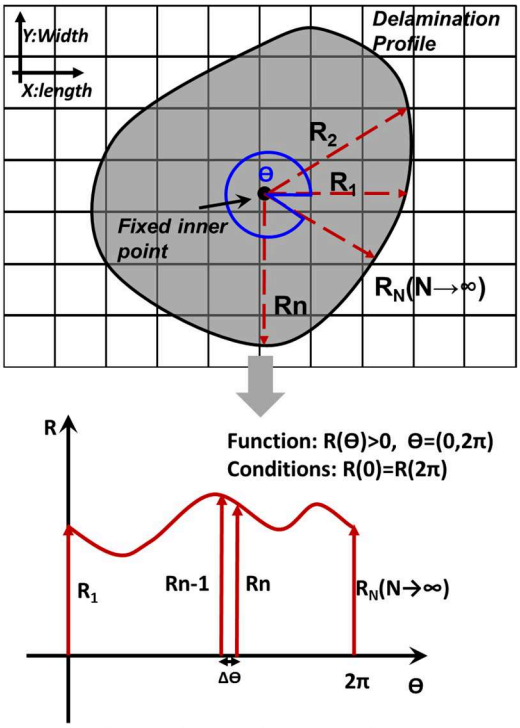

Fig. 6. Fourier series fitting radiative radius for profile parametrization

In practice, as most kinds of delamination defect have shapes with a smooth boundary, small number of coefficients are adequate to provide a good description of a wide variety of delamination profile. Typically, fewer than ten coefficients are sufficient. In other words, with this defect profile parameterizing method, a smaller set of parameters results in greater applicability to both the complexity and diversity of real delamination profiles. Applying inverse reconstruction not only improves the sizing efficiency, but also reduce the complexity and ill-posedness of inversion analysis.

B. Inversion Algorithm

Thermography inverse analysis is a typically ill-posed problem that can be addressed by the optimization method. By expressing the objective function (shown in (8)) as the residual between simulated and measured signals, the profile sizing reconstruction can be realized by searching the optimal defect parameters, which leads to the minimized objective function.

$$\psi(x) = \sum_{n=1}^{M}\left|T_n^{Sim}(x) - T_n^{mea}\right|^2 \tag{8}$$

where T_n^{mea} and T_n^{Sim} are the characteristic signals extracted from the IRT-measured and simulation images, respectively. M is the number of signals, and x is the defect parameter vector of delamination profile.

In this work, a conjunction gradient (CG) algorithm is applied to quantify the delamination profile. As mentioned in Section II. A and B, by using the proposed parameterizing strategy and fast forward simulator, the length of radiative radius *R(x, θ)* has an explicit feasible region. This can be written as constraint conditions as in (9),

$$\begin{aligned} &\textit{Constraint conditions}: \ Rmax > R(x,\theta) > 0 \\ &R(x,\theta) = \frac{1}{2}x_0 + x_n\sum_{n=1}^{N}\cos(n\theta) + \varepsilon(\theta), \qquad \theta \in [0, 2\pi] \end{aligned} \tag{9}$$

where *Rmax* is the maximum radius length to ensure that the radius cannot exceed the suspect region Ω_0 used in the fast forward simulator. Nonetheless, because of the implicit function relationship between the Fourier series coefficients and the radius length, it is hard to directly confine the Fourier series coefficients to obey the constraint conditions. Therefore, the penalty function conjunction gradient method is applied to realize the inverse defect reconstruction.

The objective function is then rewritten in (10)

$$\begin{aligned} &\min f(x) = \psi(x) + \mu^p \cdot B(x) \\ &= \sum_{n=1}^{M}\left|T_n^{Cal}(x) - T_n^{obs}\right|^2 + \sum_{j=1}^{NR}\left(\frac{\mu^p}{R_j(x)} + \frac{\mu^p}{Rmax - R_j(x)}\right) \end{aligned} \tag{10}$$

$$d_k = \begin{cases} -g_k & (k=1) \\ -g_k + \beta_k d_{k-1} & (k \geq 2) \end{cases}, \quad \beta_k^{FR} = \frac{\|g_k\|^2}{\|g_{k-1}\|^2} \tag{11}$$

where, $B(x) = \sum_{r=1}^{m} 1/q_r(x)$ denotes the interior penalty function and $q_r(x) \geq 0$, $r = 1, \cdots, m$ represents the constraint conditions. μ^p is the penalty factor and k is the iteration step. To update the parameters, the updating direction of the CG algorithm is written as (11), and gradient can be calculated by (12). In (12), $\partial T_n^{Cal}(x)/\partial x_i$ and $\partial R_j(x)/\partial x_i$ are calculated by the difference derivation method.

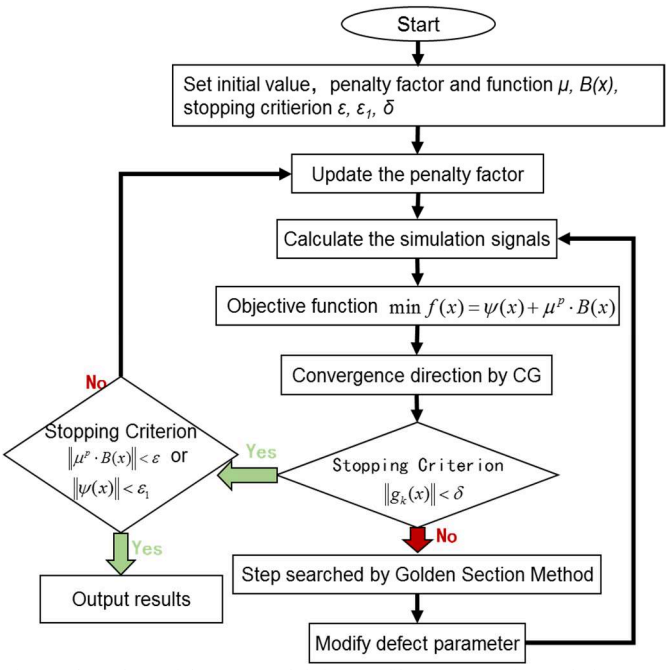

Fig. 7 Flow chart of the proposed defect profile reconstruction technique

$$\begin{aligned} g_k(x_i) = \frac{\partial f(x)}{\partial x_i} = 2\sum_{n=1}^{M}\left\{\{T_n^{Cal}(x) - T_n^{obs}\} * \frac{\partial T_n^{Cal}(x)}{\partial x_i}\right\} + \\ \mu^p \cdot \sum_{j=1}^{NR}\left(\frac{1}{\left(Rmax - R_j(x_i)\right)^2} - \frac{1}{\left(R_j(x_i)\right)^2}\right) \cdot \frac{\partial R_j(x)}{\partial x_i} \end{aligned} \tag{12}$$

Finally, an exact step search method based on the advance and retreat method and the golden section method (i.e., the 0.618 method) is adopted to guarantee the convergence speed for each iteration step.

To ensure a robust reconstruction, initial parameters such as initial defect profile and penalty factor must be properly selected. First, the interior penalty function is adopted, which indicates that the initial profile has to be selected under constraint conditions. In other words, the fixed center point in defect parametrization must be selected within the constrained area, and simultaneously in the true profile. Fortunately, this can be easily realized, because the IRT-measured image provides a clear indication of the peak value pixel location in defect area. In addition, the initial penalty factor $\mu_{k=0}^p$ has a significant impact on the convergence speed. After multiple attempts, the $\mu_{k=0}^p$ value is properly chosen to ensure a fast speed when the gradient for the objective function $\psi(x)$ is about 20-30 times the gradient for $f(x)$.

After the discussion of the major parts of the method outlined above, it should be noted that the choice of characteristic signal used in the objective function given in (8) also has a great impact on the final reconstruction results. The characteristic signal should be sensitive to defect profile and while being robust to noise. In this paper, the difference between the 1st derivative signal from the defective target and the non-defective

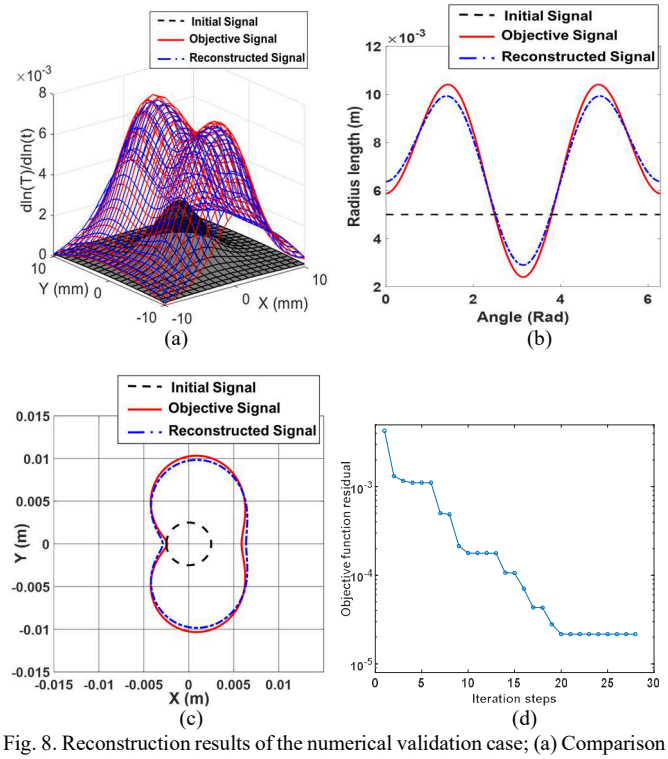

Fig. 8. Reconstruction results of the numerical validation case; (a) Comparison of characteristic signals; (b) Comparison of radius length; (c) Comparison of delamination profiles; (d) Convergence of objective function; residual

target, respectively, is selected as the characteristic signal. In pulse thermography, the 1st derivative image provides abundant defect profile information and can be easily obtained by the thermographic signal reconstruction (TSR) method [16].

So far all the components which are crucial to the delamination profile reconstruction have been carefully discussed and presented. The entire work flow for profile reconstruction can be reviewed in the chart shown in Fig. 7.

IV. VALIDATIONS

A. Validation with simulated IRT signals

In this section, to validate the proposed inverse reconstruction method, a double-layered plate model with a complex delamination was established (Fig. 4) and the corresponding inverse reconstruction code was developed. The objective delamination was set at the layer interface, and was 0.3mm in thickness with the profile shown as the red full-line in Fig. 8(c). The model was heated by pulse heat flow and the difference 1st derivative signal was selected as the characteristic signal. In this case, a model using five Fourier series coefficients model was adopted to reconstruct the objective profile. To verify the robustness of proposed method, this case selected the simulation signal of the true defect with 5% Gaussian noise as the objective signal.

Fig. 8 shows the reconstructed results and comparisons to the initial and objective defects. Fig. 8 (a), (b) and (c) show the comparisons of the characteristic signal, radiative radius length and defect profiles, respectively. The near-perfect accordance in defect profile and size demonstrates the validity of the proposed method. Fig. 8(d) presents the convergence process of the objective function: this clearly shows that the predicted profiles gradually approximate the objective, and also demonstrates the stability and robustness of the inversion algorithm.

B. Validation with measured IRT signals

1) Experimental System and Specimens

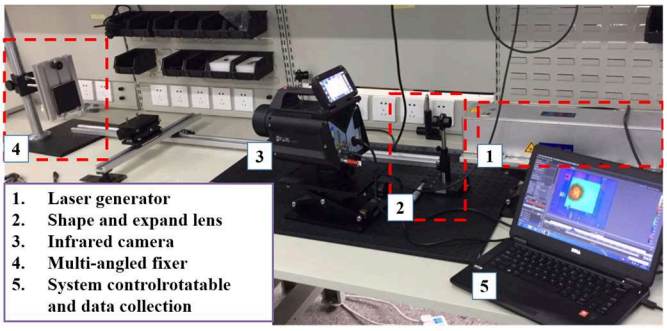

Fig. 9 Picture of the established laser thermography experiment system

To validate the developed inverse technique experimentally, a laser thermography testing system was established for inspection of delamination defects in a double layered plate. The full view of the testing system is shown in Fig. 9. The thermal images were acquired by a FLIR-A6700sc mid-wave infrared thermal camera, with a spectral range of 3.7-5.0 μm and an Indium Antimonite (InSb) detector. Table I gives the key technical specifications of the infrared camera and the laser excitation source that are the major components of the

TABLE I
EXPERIMENTS SPECIFICATION

Items	Specification
Infrared camera	Infrared range: 3.7-5.0 μm Thermal sensitivity: less than 20 mK Detector resolution: 640×512 Maximum frame rate: 60 Hz
Long pulse laser generator	NG.YAG laser, 1064nm Max 100W power Square pulse: 40 s period / 50% duty cycle
Specimen heating	20 seconds exposure time with the laser spot 50mm diameter circle homogenous laser spot
Image sampling of IR camera	60 Hz sampling rate 40 s sampling duration 2400 images captured

TABLE II
SPECIFICATIONS OF SPECIMENS

Double-layered Specimen	Sizes and materials
Al-Cu specimen	Rectangle plate with square delamination defects Height: 100 mm; Width: 100 mm Thickness: 10.5 mm Al layer Thickness: 5.5 mm Cu layer Thickness: 5.0 mm
SUS304 specimen	Rectangle plate with circle and ellipse delamination defects Height: 130 mm; Width: 130 mm Thickness: 8.3 mm First SUS304 layer Thickness: 3.3 mm Second SUS304 layer Thickness: 5.0 mm

experimental system. A 20 seconds square wave laser pulse was applied to the specimen. The laser spot was shaped to produce uniform power distribution and expanded to a of 50 mm diameter, circular heating area on the specimen. The heating area was targeted at the centre of each delamination defect in

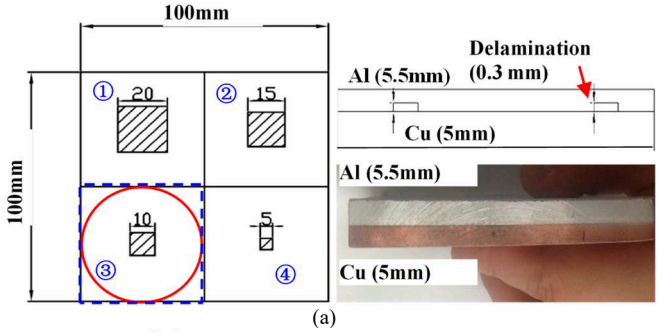

Fig. 10 Schemetic of speicmens. (a) Al-Cu double-layered specimen; (b) SUS304 double-layered specimen

the double layered specimen, shown as the red circle area in Fig. 10. The IR camera recorded the thermal images at 60 Hz frame frequency for about 40 seconds, and 2400 images were stored for each experiment. Between successive experiments, a ten-minute interval was allowed for the specimen to cool.

In experiments, to simulate delamination defects at the welding interface, two double-layered specimens with different delamination profiles were fabricated by the diffusion welding technique (see Fig. 10). The specifications of the two specimens, designated Al-Cu specimen and SUS304 specimen, respectively, are shown in Table II. Before heating, the upper surface and was black painted to reduce noise and enhance the emissivity. All the delamination defects were tested, and thermal images were obtained in the same testing environment shown in Fig. 9. The recorded thermal images were processed by subtracting an initial thermal image measured before heating. Fig.11 presents the extracted characteristic signal images of the biggest delamination in each specimen. The experimental details, extraction method and data have been carefully discussed [16].

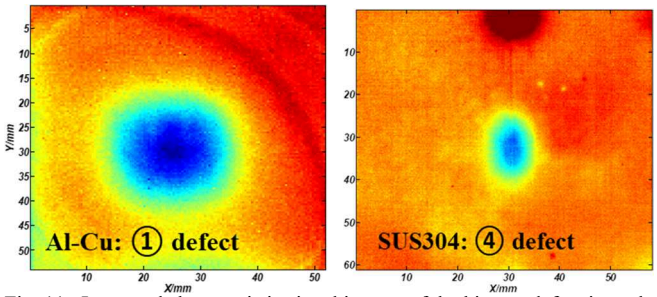

Fig. 11. Inspected characteristic signal images of the biggest defect in each specimen.

2) *Reconstructed Results*

In order to demonstrate the validity of the developed inversion reconstruction techniques for delamination profiles from IRT signals, artificial delamination defects were reconstructed. Initially, it was necessary to establish a simulation model for our specimen. Two models of the same size as the two weld specimens (Al-Cu and SUS304 specimens) were considered. (The simulation models and fast forward simulation method were earlier discussed in [29]).

In the inversion procedure, the proposed reconstruction scheme can approximate any planar complex delamination profile. Therefore, the delamination defects were represented by nine parameters of Fourier series coefficients defect models of identical thickness to the artificial defects. In addition, as the interior penalty function was adopted in inverse algorithm, and there is an ill-posedness problem in the inversion algorithm for multi-parameters reconstruction, in this study, the fixed centre point for the radiative radii in each case was set as the peak location in inspection images, which ensured that the fixed point would be inside the true profile. In addition, the starting defect profile in each case was set as a circular shape smaller than the constraint region. All computation was carried out in the computational environment of an Intel Xeon E5-2620 v3, 2.4GHz, 64GB memory, CentOS 6 and Intel FORTRAN Compiler 11.0. Under this condition, one iteration step approximately took 4.5 minutes and an entire reconstruction of 20-30steps took 1.5-2 hours.

Figs. 12 and 13 present the reconstructed results for each artificial delamination in the SUS304 and Al-Cu specimens comparing initial, reconstructed and true profiles. To demonstrate the accuracy, defect areas of reconstructed and true profiles are shown in Tables III and IV. Most of the

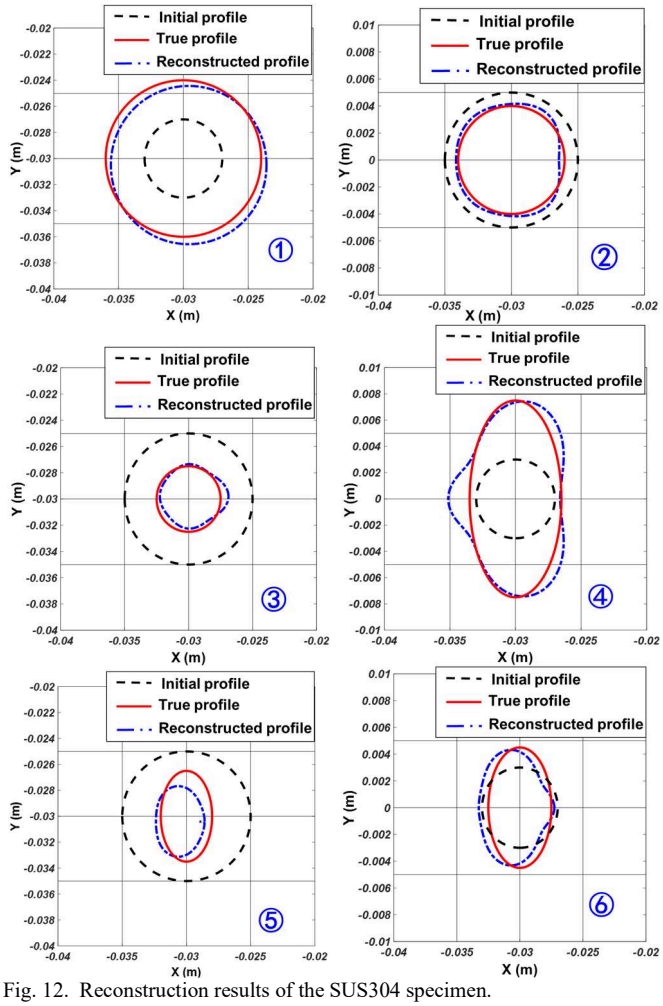

Fig. 12. Reconstruction results of the SUS304 specimen.

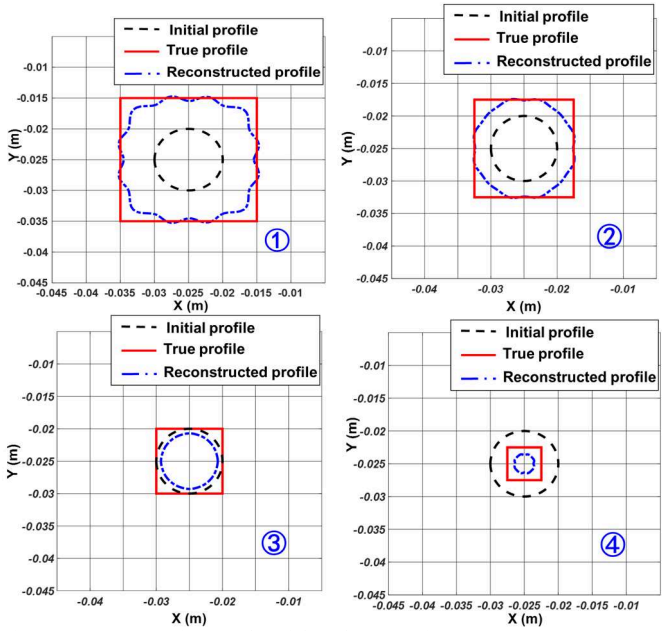

Fig. 13. Reconstruction results of the Al-Cu specimen.

reconstructed profiles display good consistency with the corresponding true profiles for defects in the SUS304 specimen. The majority of area errors are approximately on the order of 10%, with the largest still under 20%. In the cases of Al-Cu specimen, the reconstructed profiles for two smaller defects do not fully restore their original shapes, and the area error on a 5mm square delamination is over 50%. However, in the particular matter of the length and width parameters, which are the key factors for damage propagation study, the reconstructed results for the Al-Cu specimen are as nearly consistent with the information taken from the true defects, except in the case of the smallest defect. It is concluded that the proposed method is effective for most delamination, and the reconstruction accuracy is satisfactory. This demonstrates the effectiveness and efficiency of the proposed IRT inverse analysis technique for detection of delamination defects.

TABLE III
RECONSTRUCTED DEFECT AREA

Defect Number	Delamination Area of SUS304 Specimen (m^2)		
	True	Reconstructed	Error (%)
①	1.13×10^{-4}	1.17×10^{-4}	3.5%
②	5.03×10^{-5}	5.26×10^{-5}	4.6%
③	1.96×10^{-5}	1.75×10^{-5}	10.7%
④	8.25×10^{-5}	9.04×10^{-5}	9.6%
⑤	2.20×10^{-5}	1.82×10^{-5}	17.3%
⑥	3.53×10^{-5}	3.87×10^{-5}	9.6%

TABLE IV
RECONSTRUCTED DEFECT AREA

Defect Number	Delamination Area of Al-Cu Specimen (m^2)		
	True	Reconstructed	Error (%)
①	4.00×10^{-4}	3.64×10^{-4}	12.5%
②	2.25×10^{-4}	1.84×10^{-4}	18.0%
③	10.0×10^{-5}	6.70×10^{-5}	33.0%
④	25.0×10^{-6}	9.78×10^{-6}	60.8%

V. Conclusion

In this study, a quantitative reconstruction approach consisting of a novel defect parameterization strategy and an inversion algorithm was proposed for sizing complexly-shaped delamination defects employing IRT signals. The planar complex profile of delamination is crucial to conformation of the integrity of a multilayered-structure, but can only be obtained with distortion using a signal-based image processing algorithm. The proposed approach provides a model-based inversion strategy that can directly and properly reconstruct complex delamination profile without pretests and calibrations for quantitative criteria.

Furthermore, compared to a conventional inversion strategy, by proposing a new defect parameterization strategy and an updated fast forward simulation, the proposed method displays significant superiority in accurate reconstruction of a complex profile using only a small number of defect parameters, with advantages of greater speed and lower computation burden. To reduce the problem of ill-posedness in inverse reconstruction, a penalty function conjunction gradient algorithm is introduced, which enhances reconstruction robustness and efficiency. Both reconstruction results using simulated and measured IRT signals from a laser thermography experimental system proved the validity of the inversion scheme. Reconstruction results using measured signals demonstrated that the proposed method can provide a highly reliable and accurate reconstruction of defect shape and boundary.

In future work, we will seek to improve the accuracy of defect profile reconstruction. To progress this method to more realistic delamination defects, a partially-delaminated defect will be modelled, and reconstruction technique of the defect profile combined with the defect thermal diffusivity distribution will be taken into investigation.

References

[1]. M. Cheminod, L. Durante, L. Seno, and A. Valenzano, "Performance Evaluation and Modeling of an Industrial Application-Layer Firewall," *IEEE Trans. Ind. Informat*., vol. 14, no. 5, pp. 2159-2170, May, 2018.

[2]. H. Ohgaki, I. Daito, H. Zen, T. Kii, K. Masuda, T. Misawa, R. Hajima, T. Hayakawa, T. Shizuma, M. Kando, and S. Fujimoto, "Nondestructive Inspection System for Special Nuclear Material Using Inertial Electrostatic Confinement Fusion Neutrons and Laser Compton Scattering Gamma-Rays," *IEEE Trans. Nucl. Sci.*, vol. 64, no. 7, pp. 1635-1640, Jul, 2017.

[3]. Z. K. Shuai, C. Shen, X. Yin, X. Liu, and Z. J. Shen, "Fault Analysis of Inverter-Interfaced Distributed Generators With Different Control Schemes," *IEEE Trans. Power Del*., vol. 33, no. 3, pp. 1223-1235, Jun, 2018.

[4]. D. M. Tsai, S. C. Wu, and W. Y. Chiu, "Defect Detection in Solar Modules Using ICA Basis Images," *IEEE Trans. Ind. Informat*., vol. 9, no. 1, pp. 122-131, Feb, 2013.

[5]. Y. Z. He, B. L. Du, and S. D. Huang, "Noncontact Electromagnetic Induction Excited Infrared Thermography for Photovoltaic Cells and Modules Inspection," *IEEE Trans. Ind. Informat*, vol. 14, no. 12, pp. 5585-5593, Dec, 2018.

[6]. X. L. Bai, Y. M. Fang, W. S. Lin, L. P. Wang, and B. F. Ju, "Saliency-Based Defect Detection in Industrial Images by Using Phase Spectrum," *IEEE Trans. Ind. Informat*., vol. 10, no. 4, pp. 2135-2145, Nov, 2014.

[7]. C. Piciarelli, D. Avola, D. Pannone, and G. L. Foresti, "A Vision-Based System for Internal Pipeline Inspection," *IEEE Trans. Ind. Informat*., vol. 15, no. 6, pp. 3289-3299, Jun, 2019.

[8]. Y. Park, and I. S. Kweon, "Ambiguous Surface Defect Image Classification of AMOLED Displays in Smartphones," Ieee Transactions on Industrial Informatics, vol. 12, no. 2, pp. 597-607, Apr, 2016.

[9]. C. Benedek, O. Krammer, M. Janoczki, and L. Jakab, "Solder Paste Scooping Detection by Multilevel Visual Inspection of Printed Circuit Boards," *IEEE Trans. Ind. Electron.,* vol. 60, no. 6, pp. 2318-2331, Jun, 2013.

[10]. Y. Li, B. Yan, D. Li, H. Q. Jing, Y. L. Li, and Z. M. Chen, "Pulse-modulation eddy current inspection of subsurface corrosion in conductive structures," *NDT&E Int*., vol. 79, pp. 142-149, Apr, 2016.

[11]. M. K. Yucel, S. Fateri, M. Legg, A. Wilkinson, V. Kappatos, C. Selcuk, and T. H. Gan, "Coded Waveform Excitation for High-Resolution Ultrasonic Guided Wave Response," *IEEE Trans. Ind. Informat*., vol. 12, no. 1, pp. 257-266, Feb, 2016.

[12]. C.X. Pei, T.H. Liu, H.E. Chen, and Z.M. Chen, 'Inspection of delamination defect in first wall with a flexible EMAT-scanning system', *Fusion Eng. Des.*, vol. 136, pp. 549-553, Nov, 2018

[13]. V. A. Udod, Y. Van, S. P. Osipov, S. V. Chakhlov, E. Y. Usachev, M. B. Lebedev, and A. K. Temnik, "State-of-the Art and Development Prospects of Digital Radiography Systems for Nondestructive Testing, Evaluation, and Inspection of Objects: a Review," *Russ. J Nondestruct*., vol. 52, no. 9, pp. 492-503, Sep, 2016.

[14]. G. W. Hwang, and J. U. Cho, "A Study on Mechanical Behavior Occurred at the Adhesive Interface Delamination of Jointed Structure," *Int. J Precis. Eng. Man*., vol. 18, no. 3, pp. 381-387, Mar, 2017.

[15]. J. A. Pascoe, R. C. Alderliesten, and R. Benedictus, "On the relationship between disbond growth and the release of strain energy," *Eng. Fract. Mech.*, vol. 133, pp. 1-13, Jan, 2015.

[16]. H. C. Liu, C. X. Pei, J. X. Qiu, and Z. M. Chen, "Inspection of Delamination Defect in First Wall Panel of Tokamak Device by Using Laser Infrared Thermography Technique," *IEEE Plasma Sci*., vol. 46, no. 7, pp. 2699-2707, Jul, 2018.
[17]. J. X. Qiu, C. X. Pei, H. C. Liu, Z. M. Chen, and K. Demachi, "Remote inspection of surface cracks in metallic structures with fiber-guided laser array spots thermography," *NDT&E Int*., vol. 92, pp. 213-220, Dec, 2017.
[18]. S. Hwang, Y. K. An, J. M. Kim, and H. Sohn, "Monitoring and instantaneous evaluation of fatigue crack using integrated passive and active laser thermography," *Opt. Laser Eng*., vol. 119, pp. 9-17, Aug, 2019.
[19]. J. Moran, and N. Rajic, "Remote line scan thermography for the rapid inspection of composite impact damage," *Compos. Struct*., vol. 208, pp. 442-453, Jan 15, 2019.
[20]. S. C. Sun, H. Qi, X. Y. An, Y. T. Ren, Y. B. Qiao, and L. M. Ruan, "Non-destructive testing of ceramic materials using mid-infrared ultrashort-pulse laser," *Appl. Phys. B-Lasers O*., vol. 124, no. 4, Apr, 2018.
[21]. S. M. Shepard, and M. F. Beemer, "Advances in thermographic signal reconstruction", SIC: SPIE, 2015.
[22]. S. J. Xie, Z. M. Chen, T. Takagi, and T. Uchimoto, "Quantitative non-destructive evaluation of wall thinning defect in double-layer pipe of nuclear power plants using pulsed ECT method," *NDT&E Int*., vol. 75, pp. 87-95, Oct, 2015.
[23]. X. J. Wang, S. J. Xie, and Z. M. Chen, "An Efficient Numerical Scheme for Sizing of Cavity Defect in Metallic Foam from Signals of DC Potential Drop Method," *IEEE Trans. Magn*., vol. 50, no. 2, Feb, 2014.
[24]. T. Aujeszky, G. Korres and M. Eid, "Measurement-Based Thermal Modeling Using Laser Thermography", *IEEE Trans. Instrum. Meas.*, vol. 67, no. 6, pp. 1359-1369, 2018.
[25]. J. L. Gong, J. Y. Liu, F. Wang, and Y. Wang, "Inverse heat transfer approach for nondestructive estimation the size and depth of subsurface defects of CFRP composite using lock-in thermography," *Infrared Phys. Technol.*, vol. 71, pp. 439-447, Jul, 2015.
[26]. R. Richter, C. Maierhofer, and M. Kreutzbruck, "Numerical method of active thermography for the reconstruction of back wall geometry," *NDT&E Int*., vol. 54, pp. 189-197, Mar, 2013.
[27]. Z. M. Chen, N. Yusa, M. Rebican, and K. Miya, "Inversion techniques for eddy current NDE using optimization strategies and a rapid 3D forward simulator," *Int. J Appl. Electromagn*., vol. 20, no. 3-4, pp. 179-187, 2004.
[28]. H. C. Liu, S. J. Xie, C. X. Pei, and Z. M. Chen, "Numerical simulation method for IR thermography NDE of delamination defect in multilayered plate," *Int. J Appl. Electromagn*., vol. 52, no. 1-2, pp. 381-389, 2016.
[29]. H. C. Liu, S. J. Xie, C. X. Pei, J. X. Qiu, Y. Li, and Z. M. Chen, "Development of a Fast Numerical Simulator for Infrared Thermography Testing Signals of Delamination Defect in a Multilayered Plate," *IEEE Trans. Ind. Informat*., vol. 14, no. 12, pp. 5544-5552, Dec, 2018.
[30]. X. J. Wang, S. J. Xie, Y. Li, and Z. M. Chen, "Efficient numerical simulation of DC potential drop signals for application to NDT of metallic foam," *COMPEL*, vol. 33, no. 1-2, pp. 147-156, 2014.
[31]. Z. F. Tong, S. J. Xie, X. D. Li, C. X. Pei, Z. M. Chen and Y. Z. He, "Efficient numerical simulation of eddy current pulsed thermography NDT signals based on FEM-BEM method and energy equivalent principle", *Infrared Phys. Technol.*, vol. 101, pp. 138-145, 2019.

Haochen Liu received his D.Eng. degree from Xi'an Jiaotong University, Xi'an, China, in 2018.

He is currently a Research Fellow in Industrial Inspection at Cranfield University, Cranfield, U.K. His research interests include in the simulations and experiments for thermal transfer problems, the theory and application of Infrared Thermography Non-destructive testing (IR-NDT), thermal image processing and inverse problems in IR-NDT.

Cuixiang Pei received his Ph.D. degree from The University of Tokyo, Tokyo, Japan, in 2012.

He is currently the Associate Professor in the Department of Engineering Mechanics, Xi'an Jiaotong University, Xi'an, China. His current research interests include development and application of new NDT methods with using EMAT, laser ultrasonic testing, and laser thermography testing.

Shejuan Xie received the B.Eng. and M.Eng. degree in applied mechanics from Xi'an Jiaotong University, Xi'an, China, in 2006 and2009, respectively, and the D.Eng. degree in bio-robotics from Tohoku University, Sendai, Japan, in 2012.

Since 2013, she has been an Associate Professor in the Department of Engineering Mechanics, Xi'an Jiaotong University. Her current research interests include electromagnetic, ultrasonic, thermography nondestructive evaluation and applied electromagnetics and mechanics.

Yong Li (SM'13) received the Ph.D. degree from Newcastle University, Newcastle upon Tyne, U.K, in 2009.

He is currently an Associate Professor of Electromagnetic Sensors for Nondestructive Evaluation (NDE) with the School of Aerospace, Xi'an Jiaotong University, Xi'an, China. His current research interests include finite element simulations and analytical modeling for electromagnetic problems, electromagnetic nondestructive testing and evaluation, 3-D magnetic field measurement using magnetic sensors and arrays, signal processing and feature extraction techniques, etc.

Yifan Zhao (SM' 16) was born in Zhejiang, China. He received the Ph.D. degree in automatic control and system engineering from The University of Sheffield U.K., in 2007.

He is currently a Senior Lecturer in Data Science with Cranfield University. His research interests include computer vision for automated vehicles, super resolution, active thermography, and nonlinear system identification.

Zhenmao Chen is the Professor in the Department of Engineering Mechanics, Xi'an Jiaotong University. He received his Ph.D. degree from The University of Tokyo, Tokyo, Japan, in 1998.

He is currently a Professor in the Department of Engineering Mechanics, Xi'an Jiaotong University, Xi'an, China. His current research interests include in the areas of strength and vibration problems due to electromagnetic force, theory and application of electromagnetic NDT, and inverse problems in NDT.

Inversion technique for quantitative infrared thermography evaluation of delamination defects in multilayered structures

Liu, Haochen

2019-10-31

Liu H, Pei C, Xie S, et al., (2020) Inversion technique for quantitative infrared thermography evaluation of delamination defects in multilayered structures. IEEE Transactions on Industrial Informatics, Volume 16, Issue 7, July 2020, pp. 4592-4602

https://doi.org/10.1109/TII.2019.2950808